Density matrix renormalization group algorithm for Bethe lattices of spin-$\frac{1}{2}$ or spin-1 sites with Heisenberg antiferromagnetic exchange

Manoranjan Kumar,[1,2,*] S. Ramasesha,[2] and Zoltán G. Soos[1]

[1]*Department of Chemistry, Princeton University, Princeton, New Jersey 08544, USA*

[2]*Solid State and Structural Chemistry Unit, Indian Institute of Science, Bangalore 560012, India*

(Received 28 October 2011; revised manuscript received 3 March 2012; published 6 April 2012)

A density matrix renormalization group (DMRG) algorithm is presented for the Bethe lattice with connectivity $Z = 3$ and antiferromagnetic exchange between nearest-neighbor spins $s = 1/2$ or 1 sites in successive generations g. The algorithm is accurate for $s = 1$ sites. The ground states are magnetic with spin $S(g) = 2^g s$, staggered magnetization that persists for large $g > 20$, and short-range spin correlation functions that decrease exponentially. A finite energy gap to $S > S(g)$ leads to a magnetization plateau in the extended lattice. Closely similar DMRG results for $s = 1/2$ and 1 are interpreted in terms of an analytical three-site model.

DOI: 10.1103/PhysRevB.85.134415 PACS number(s): 75.10.Jm, 71.10.Fd, 05.30.−d, 05.10.Cc

I. INTRODUCTION

Dendrimers have been extensively explored over the past two decades, both experimentally and theoretically. Dendrimers are macromolecules with repetitive branches attached to a central core or focal point.[1,2] Three parameters (b, Z, g) characterize the dendrimer lattice model in Fig. 1: the number of branches b attached to the focal point, the connectivity Z of a site, and the number of generations g. Many natural systems are dendrimers, and molecular engineering can produce custom dendrimers with constituents that range from carbon-based molecules[3] to organometallic compounds.[4,5] Potential applications include drug delivery for chemotherapy,[3] gene therapy,[6] magnetic resonance imaging as contrast agents based on superparamagnetism,[7] and molecular recognition.[8]

Bethe lattices (BLs) or Cayley trees are theoretical models of dendrimers and attractive approximations of solid-state systems. We consider in this paper superparamagnetic dendrimers based on sites with unpaired spins. BLs are fundamentally one-dimensional (1D) systems, without any closed loops, that can be divided by cutting any bond. Their distinctive feature is exponential growth with g. Half of the sites for the BL with $Z = 3$ in Fig. 1 are on the surface in generation g. BLs are bipartite: all nearest-neighbor (NN) bonds in Fig. 1 are between sites in even and odd g that define two sublattices with different numbers of sites. The BL has open boundary conditions, a focal point at $g = 0$, and an arbitrarily large boundary g. General theorems apply for the spectrum free electrons[9] with NN transfer t in a BL or for spins[10] with NN Heisenberg exchange $J > 0$. Three parameters generate a rich variety of BL(b, Z, g). In dynamical mean-field theory,[11] the BL density of states with infinite connectivity is used as an initial guess for the density of states in higher dimensions. BLs are models for strongly correlated systems,[12] alloys,[13] and disordered systems.[14] The present study addresses antiferromagnetic (AF) Heisenberg exchange $J > 0$ in the BL with $b = Z = 3$,

$$H(g) = \sum_{\langle i,j \rangle} J \vec{s}_i \cdot \vec{s}_j. \tag{1}$$

The sum $\langle i, j \rangle$ is over all NN for either $s = 1/2$ or $s = 1$ sites. BL-Ising models limited to $s_i^z s_j^z$ interactions have been used to study finite spin glasses.[15] The electronic properties of correlated BL models still pose many challenges.

Recent advances in numerical techniques and computational resources have been applied to BL models. Methods include exact diagonalization (ED), quantum Monte Carlo (QCM),[16] and density matrix renormalization group (DMRG).[17] DMRG is particularly well suited for 1D systems such as Hubbard or extended Hubbard models, t-J models, and Heisenberg or related spin models. DMRG yields accurate properties for the ground state (gs) or low-energy excited states.[18–21] The DMRG challenge for a BL is the large number of surface sites in Fig. 1. Otsuka[22] applied DMRG to the BL, Eq. (1), with $s = 1/2$ sites and axially anisotropic NN exchange (XXZ model). Friedman[23] presented another DMRG algorithm for Eq. (1) with $s = 1/2$. Lepetit *et al.*[24] used essentially the same algorithm to treat the Hubbard model version of Eq. (1) that reduces to $J = 4t^2/U$ for $s = 1/2$ when the on-site repulsion U is large compared to NN electron transfer t. They also solved analytically the Hückel or tight-binding model with $U = 0$.

DMRG is a truncation procedure in which insignificant degrees of freedom of the system block, the right or left block in a chain, are discarded at each step with increasing system size. In 1D chains, the superblock consists of two blocks with dimension m and two sites with p degrees of freedom. The superblock dimension is $m^2 \times p^2$, with $p = 2s + 1$ in spin systems. The DMRG procedure is equivalent to a matrix product state (MPS) approach. The MPS method is found to be useful in attempts to extend the DMRG method to higher dimension.[25] The superblock of BL$(3,3,g)$ has three blocks and hence goes as m^3. More branches b increase the computational requirements. Otsuka[22] used four blocks and two new sites for BL$(3,3,g)$ with $p = 2$ ($s = 1/2$). His superblock increased as $m^4 \times p^2$. The Friedman algorithm[23] with $b = 3$ and four new sites yields a superblock dimension of $m^3 \times p^4$. The DMRG algorithm in Sec. II has a superblock dimension $m^3 \times p$ or, more generally, $m^b \times p$, which makes $s = 1$ sites accessible.

The paper is organized as follows. Section II presents and tests our algorithm. Section III reports results for the BL in Fig. 1 and Eq. (1) up to $g = 11$ for $s = 1/2$ and 1 sites, and up to $g > 20$ for $\langle s_0^z \rangle$ at the focal point. We obtain the gs energy per

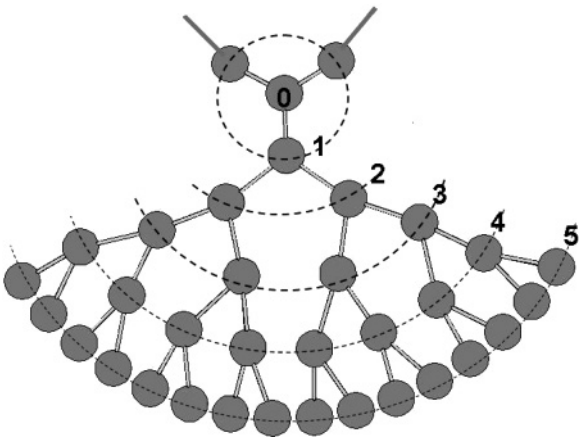

FIG. 1. One arm of a Bethe lattice with $b = Z = 3$ and $g = 5$. The other two arms are shown to generation $g = 1$; g also represents the distance from the focal point.

site, the energy gap Δ that governs the gs magnetization, and gs expectation values of s_n^z for $n \leqslant g$. We find spin correlation functions between the focal point and other sites and their convergence with increasing g. Section IV relates the DMRG results to a simple analytical model with localized states, to previous DMRG studies, and to the question of long-range order in the infinite BL.

II. DMRG ALGORITHM

In this section, we present a DMRG algorithm for the BL in Fig. 1 with $b = Z = 3$. The principal change is how the lattice is grown. The total number of sites in BL(3,3,g) is

$$N_T(g) = 1 + 3(2^g - 1). \tag{2}$$

The first step in Fig. 2 contains four sites. Sites A, B, and C are blocks each of whose size is 2^{g-1} at generation g. The focal point D is the new site added at each step. As shown in Fig. 2, each block $A = B = C$ contains three sites

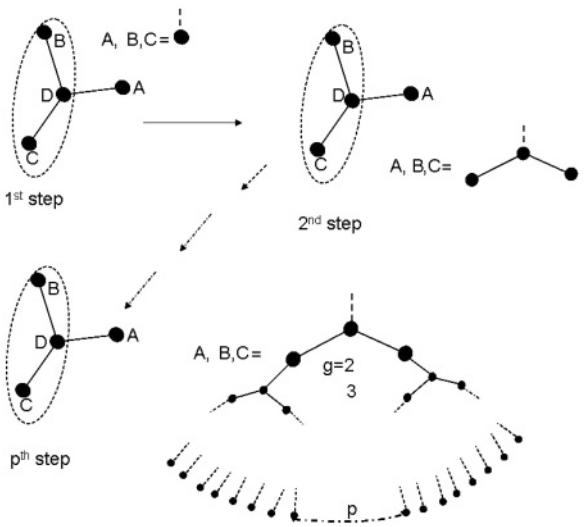

FIG. 2. Schematic representation of BL growth from $g = 1$ at step 1 to $g = p$ at step p. The blocks $A = B = C$ at step g are given by Eq. (2). The focal point D is the new site added at each step.

in the second step for $g = 2$. Growth at step $g = 2,3,\ldots$ is schematically represented as

$$A_{g+1} = \begin{array}{ccc} & D_g & \\ A_g & & A_g \end{array} \tag{3}$$

D_g is connected to the focal point D at step $g + 1$. The next step gives blocks of seven sites at $g = 3$, and so on up to the BL with $N_T(g)$ sites. The procedure for BL(3,3,g) holds for other b and Z.

The infinite DMRG algorithm for the BL proceeds along largely standard lines:[17] (i) Start with the superblock matrix of four sites and find the eigenvalues of H. (ii) Use the eigenvectors of the superblock to construct the density matrix of the new blocks A_{g+1}, initially for $g = 1$. Keep the eigenvectors of the m largest eigenvalues, with m chosen as discussed below. The density matrix dimension is $m^2 \times p$, where m and p refer to the block and degrees of freedom of the new site. Full diagonalization of the density matrix is carried out separately for large m in sectors with different total S^z. (iii) Renormalize the Hamiltonian of the new blocks and the operators that are necessary for the next step. These steps follow conventional DMRG.[17] (iv) Construct the next $(g + 1)$ superblock from the three renormalized blocks A_{g+1} and the new site. Diagonalize the matrix and retain the m lowest eigenvalues and eigenvectors. Repeat steps (ii)–(iv) until the desired system size is reached.

The superblock dimension of $m^3 \times p$ makes possible larger m, which increases the accuracy, and larger $p = 2s + 1$. We can use $m = 60$ without much computational effort and find 10^{-13} or less for the weight of the discarded eigenvalues of blocks. DMRG is a variational method. Energies and correlation functions for given size g converge better for finite DMRG.[17] We followed the standard approach of sweeping back and forth through different blocks. Care has to be taken in designing the finite DMRG algorithm due to the complex structure of the BLs.

We constructed the density matrix with equal weight for the lowest two eigenstates. As a first test of accuracy, we performed ED on BL(3,3,3) with 22 sites $s = 1/2$ and on BL(3,3,2) with 10 sites $s = 1$. There are 2^{22} and 3^{10} spin states, respectively. DMRG results with increasing m must eventually converge to ED. The evolution of the gs energy per site, $\delta\epsilon_0 = \epsilon_0(m) - \epsilon_0(\text{ED})$, with m is shown in Table I for the 22-site systems. Also shown are the evolution of $\delta\langle s_3^z\rangle$ and the spin correlation $\delta\langle s_0^z s_3^z\rangle$ between the focal point and the boundary. DMRG with $m = 50$ is quantitative here. The

TABLE I. The difference δX between ED and DMRG with increasing m for BL(3,3,3) with $s = 1/2$ sites, where X is the gs energy per site ϵ_0, Δ is the excitation energy, $\langle s_3^z\rangle$ is the boundary spin, and $\langle s_1^z s_3^z\rangle$ is the spin correlation.

m	$\delta\epsilon \times 10^9$	$\delta\Delta \times 10^4$	$\delta\langle s_3^z\rangle \times 10^4$	$\delta\langle s_0^z s_3^z\rangle \times 10^5$
10	2670.8	42.593	89.48	−1.193
20	560.08	41.441	0.030	−0.722
30	552.99	41.212	0.031	−0.801
50	0.001	0.0008	0.003	−0.0001

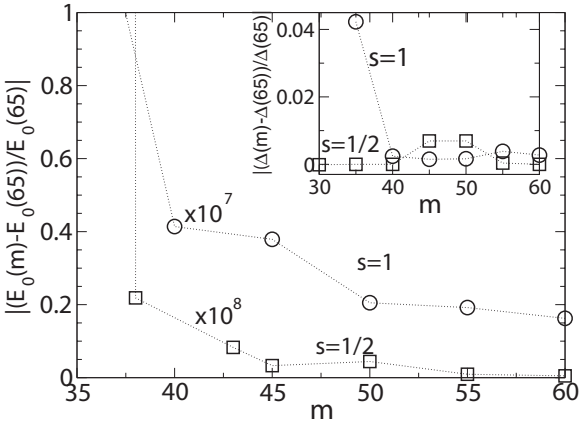

FIG. 3. Ground-state energy E_0 of spins 1/2 and 1 in a large BL(3,3,10) as a function of m relative to $m = 65$. The inset shows the m dependence of the energy gap Δ to the ground state with $S^z = S(10) + 1$.

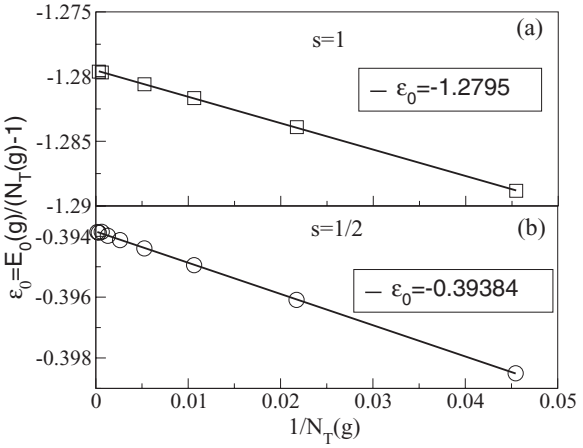

FIG. 4. Ground-state energy ϵ_0 per bond of the BL, Eq. (1), with $s = 1/2$ and 1 sites, $g \leqslant 11$ generations, and $N_T(g)$ sites. Linear extrapolation gives ϵ_0 of the extended BL.

Friedman algorithm whose superblock increases as $m^3 \times p^4$ is limited to $m \approx 30$ and returns[23] $\delta\epsilon_0 = 2.2 \times 10^{-6}$ with $m = 29$ for infinite DMRG, which is comparable to $m = 10$ in Table I. DMRG with increasing m also agrees quantitatively with ED for $s = 1$ sites.

We chose $m = 60$ on the basis of BL calculations for large systems with $g = 10$. Figure 3 shows the evolution of $\epsilon_0(m)/\epsilon_0(65)$ with m for $s = 1/2$ and 1 sites. Although $s = 1$ converges an order of magnitude more slowly, $m > 40$ is adequate in either case. Preliminary results indicate still slower convergence for $s = 3/2$ sites. The inset of Fig. 3 shows the slower, and not monotonic, evolution of the energy gap $\Delta(m)/\Delta(65)$. This is not unexpected since Δ is the difference between two extensive quantities: the absolute gs with $S = S(g)$ and the lowest state with $S' = S + 1$.

We followed the first excited state in $S^z = S(g)$ with similar results. We kept $m = 60$ and did eight sweeps of finite DMRG for the results in Sec. III. We estimate that the gs energy, spin densities, and spin correlation functions are accurate to four to five decimal places in larger systems, while energy gaps are accurate to two to three places.

III. RESULTS FOR BL WITH $s = 1/2$ AND 1

In general, a BL of N_T sites has $N_T - 1$ bonds, since only the focal point is not connected to a site with lower g. The gs energy per bond of BL(3,3,g) is

$$\epsilon_0(g) = E_0(g)/[N_T(g) - 1], \tag{4}$$

where E_0 is the gs energy and N_T is given in Eq. (2). Figure 4 shows $\epsilon_0(g)$ for $s = 1/2$ and 1 sites up to $g = 10$. There is very little size dependence. The extended $s = 1/2$ and 1 systems have $\epsilon_0 = -0.393\,84$ and -1.2795, respectively.

The gs has a total z component of spin $S^z(g) = 2^g s$. Equation (1) conserves S, and either a half-filled band or Heisenberg exchange yields $S(g) = 2^g s$. Finite g corresponds to a superparamagnetic BL with $2S(g) + 1$ degeneracy in S^z, and all calculations are performed in the $S^z = S(g)$ sector.

The gap $\Delta(g)$ to the gs in the $S^z = S(g) + 1$ sector governs the gs magnetization. The evolution of $\Delta(g)$ with $N_T(g)$ is shown in Fig. 5. The substantial gap of the extended system is discussed in Sec. IV. We also found doubly degenerate excitations $\Delta'(g)$, comparable to $\Delta(g)$, in the $S^z(g)$ sector for both $s = 1/2$ and 1. The C_3 symmetry (not used) of the BL leads naturally to E states. Since we compute S^z rather than S, the gs automatically appears also in sectors with $S^z < S^z(g)$. The energy of the second and third excited states for $S^z = S^z(g) - 1$ decreases with $N_T(g)$, and these excitation energies vanish in the extended system within our numerical accuracy.

The gs expectation values of $\langle s_p^z \rangle$ in generation p are listed in Table II for the BL with $g = 10$. The $g = 9$ and 11 results are almost the same. The gs has long-range order (LRO) that corresponds to staggered magnetization in successive generations. The largest $\langle s_p^z \rangle$ is at the boundary, $p = g$. The smallest magnitude is at $p = g - 1$ next to the boundary, and $|\langle s_n^z \rangle|$ near the focal point become equal for large g. The convergence of $|\langle s_0^z \rangle|$ to 0.348 is shown in Fig. 6 up to $g = 26$, a huge BL of 3×2^{26} sites, and agrees with the previous estimate of 0.35.[24] The $s = 1$ limit up the $g = 24$ is $|\langle s_0^z \rangle| = 0.83$, and the staggered magnetization of both gs becomes constant near the focal point for $g > 10$. By contrast,

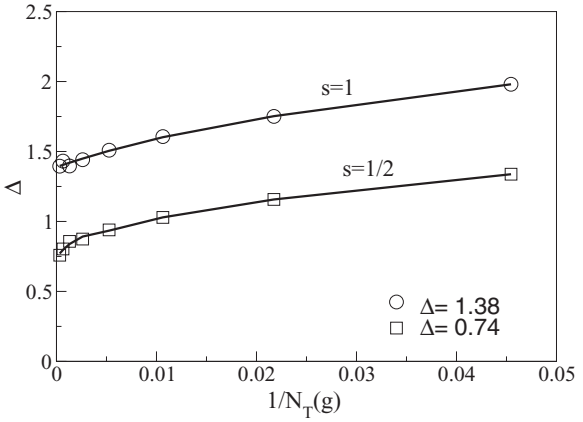

FIG. 5. Size dependence of the energy gap Δ to $S^z = S(g) + 1$ for the BL, Eq. (1), with $s = 1/2$ and 1 sites, $g \leqslant 11$, and $N_T(g)$ sites.

TABLE II. Ground-state expectation values of $\langle s_p^z\rangle$ and $\langle \vec{s}_{p-1}\cdot\vec{s}_p\rangle$ for $s = 1/2$ and 1 sites in BL(3,3,10). The focal point and boundary are $p = 0$ and 10, respectively.

	$s = 1/2$		$s = 1$	
p	$\langle s_p^z\rangle$	$\langle \vec{s}_{p-1}\cdot\vec{s}_p\rangle$	$\langle s_p^z\rangle$	$\langle \vec{s}_{p-1}\cdot\vec{s}_p\rangle$
0	0.347		0.829	
1	−0.345	−0.359	−0.828	−1.214
2	0.347	−0.361	0.828	−1.214
3	−0.342	−0.357	−0.826	−1.213
4	0.348	−0.364	0.826	−1.215
5	−0.332	−0.350	−0.817	−1.208
6	0.348	−0.371	0.820	−1.218
7	−0.307	−0.334	−0.789	−1.191
8	0.356	−0.392	0.816	−1.238
9	−0.249	−0.289	−0.691	−1.104
10	0.393	−0.456	0.872	−1.397

a half-filled BL of a free electron has $\langle s_0^z\rangle = 2/(g+1)$ for odd g and $\langle s_0^z\rangle = 0$ for even g or in the extended system.

Table II also lists the gs expectation values of $\langle \vec{s}_{p-1}\cdot\vec{s}_p\rangle$ in successive generations of BL(3,3,10) with $s = 1/2$ and 1 sites. The $g = 9$ and 11 values are similar. Variations of $\langle \vec{s}_{p-1}\cdot\vec{s}_p\rangle$ at g and $g-1$ are reduced near the focal point. The BL-Ising model has $\langle s_p^z\rangle = (-1)^p s$ and $\langle s_{p-1}^z s_p^z\rangle = -s^2$. Table II shows that $s = 1$ is closer to the Ising model than $s = 1/2$, where quantum fluctuations are larger.

We define radial spin correlation functions as

$$C(r) = (-1)^r\left(\langle \vec{s}_0\cdot\vec{s}_r\rangle - \langle s_0^z\rangle\langle s_r^z\rangle\right) \tag{5}$$

with $r = 1,2,\ldots,g$. The mean-field contribution is explicitly excluded. As seen in Fig. 7, $C(r)$ decreases as $\exp(-\alpha r)$ with $\alpha = 0.80$ for both $s = 1/2$ and 1. Accurate DMRG makes it possible to compute small $C(r)$ up to $r \approx 10$. The inset shows the related correlation function $C^z(r)$ with $\langle s_0^z s_r^z\rangle$ instead of the dot product, which decreases even faster. Although the model has isotropic exchange, the gs has $S = 2^g s$ and $C(r)$ in the $S^z = 2^g s$ sector is almost completely due to transverse spin components. Since the number of boundary sites goes as $n(g) = 1.5\exp(g\ln 2)$, we have $n(g)C(g) \to 0$ for large g.

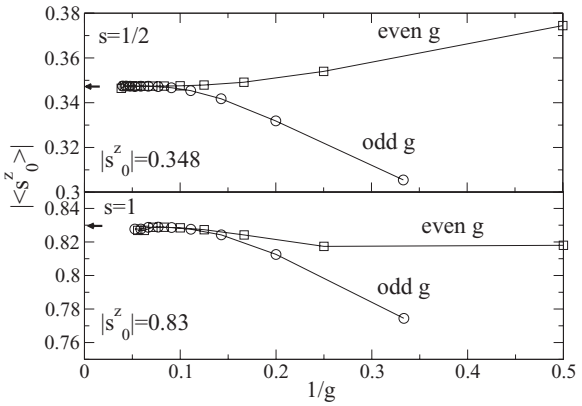

FIG. 6. Magnitude of $\langle s_0^z\rangle$ at the focal point of a BL up to $g = 26$ generations for $s = 1/2$ and up to $g = 24$ for $s = 1$ sites. Even and odd g form separate series that merge at large g.

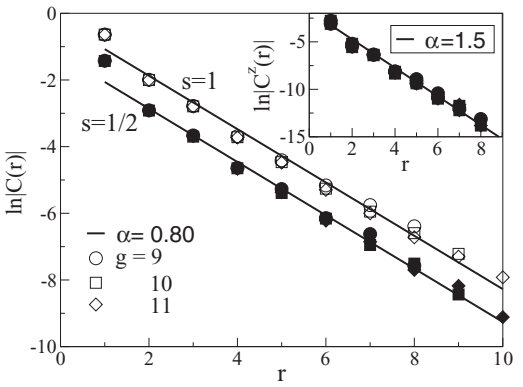

FIG. 7. Spin correlation functions $C(r)$ in Eq. (5) between the focal point and generation $r \leqslant g$ in BLs with $g = 9$, 10, and 11 and $s = 1/2$ and 1 sites. The inset shows the z component, $C^z(r)$.

The gs degeneracy is lifted when an applied magnetic field h is added to Eq. (1). The lowest Zeeman level goes as $-hS(g)$. With increasing h, the gs becomes the lowest Zeeman level of a state with $S^z > S(g)$, an excited state at $h = 0$. When $S^z = S(g)+1$, the crossover field is related to the zero-field energy in the two sectors,

$$h = \Delta(g) = \{E_0[S(g)+1] - E_0\}/J. \tag{6}$$

The first crossover may be to a state with higher S^z, when Eq. (6) has a multiple of h. The gs magnetization per $s = 1/2$ site of BL(3,3,g) is shown in Fig. 8 for $g = 3$, 4, and 5. The first jump is to $S^z = S(g) + 1$. Complete alignment at large h leads to $M = 1/2$ in reduced units. The extended BL with infinite g has a magnetic gs with $M = 1/6$ at $h = 0$ and an initial increase at Δ marked with an arrow in Fig. 8.

IV. DISCUSSION

DMRG results for $H(g)$ in Eq. (1) are similar for BLs with $s = 1/2$ and 1 sites in Fig. 1. The gs has $S(g) = 2^g s$ as expected on general grounds. The larger sublattice has $N_A(2) = 2^{g+1} - 1$ sites and the smaller has $N_B(g) = 2^g - 1$ sites. The difference $N_A(g) - N_B(g)$ is 2^g. As seen in Table II, the gs has staggered magnetization with LRO and AF

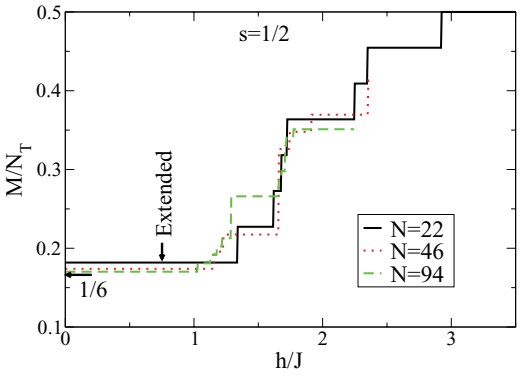

FIG. 8. (Color online) Exact magnetization M per site of BL(3,3,3) with $s = 1/2$ sites as a function of applied field h. The $g = 4$ and 5 magnetization is DMRG up to finite h. The extended BL has an $M = 1/6$ plateau up to $h = \Delta$, the gap shown in Fig. 5.

spin correlations in successive generations. Spin correlation functions $C(r)$ in Fig. 8 decay rapidly and exponentially. Magnetization has a substantial gap $\Delta(g)$ that remains finite in the extended $s = 1/2$ or 1 system.

We interpret these results in terms of a simple analytical approximation. We partition $H(g)$ with $J = 1$ in Eq. (1) as $H = H_0 + V$,

$$H_0 = N_B(g)h(3), \quad h(3) = \vec{s}_2 \cdot (\vec{s}_1 + \vec{s}_3). \tag{7}$$

The trimer $h(3)$ is elementary and H_0 accounts for exactly 2/3 of the exchanges. For example, the outermost two generations of BL(3,3,5) in Fig. 1 contain eight trimers per arm. Each $s = 1/2$ trimer has a gs with $s = 1/2$ at $e_0 = -1$, another doublet at $e = 0$, and a quartet, $s = 3/2$, at $e = 1/2$. The gs of an $s = 1$ trimer is $e_0 = -3$. The perturbation V contains an extra site q in the larger sublattice and remaining exchanges. Each of $N_A(q)$ choices of q uniquely defines the sites of $N_B(g)$ trimers. The middle and end sites are necessarily in the smaller and larger sublattice, respectively, and all exchanges in V are between a middle and end site. There is only one kind of trimer-trimer or trimer-q interaction.

The gs energy of H_0 for $s = 1/2$ and 1 sites is $-N_B(g)$ and $-3N_B(g)$, respectively. Spin correlation functions of adjacent sites for $s = 1/2$ and 1 are

$$\langle \vec{s}_1 \cdot \vec{s}_2 \rangle = -1/2, -3/2. \tag{8}$$

The spin densities of the central and terminal sites for $s = 1/2$ are

$$2\langle s_2^z \rangle = -1/3, \quad 2\langle s_1^z \rangle = 2/3. \tag{9}$$

The corresponding spin densities for $s = 1$ are -1 in the middle and 3/2 at the ends. The gs of H_0 is a product over trimers and the spin at q,

$$|\Psi^{(0)}(q,g)\rangle = |\alpha_q\rangle \prod_{j=1}^{N_B(g)} |\psi_j\rangle. \tag{10}$$

First-order perturbation theory in V lifts the degeneracy between q in generations g and $<g$.

Site q is a $1/N_T$ correction for large g. The energy per site of the infinite BL is, to first order in V,

$$\langle \Psi^{(0)}|H|\Psi^{(0)}\rangle/3N_B(g) = \epsilon_0(s)/3 + \langle s_1^z \rangle \langle s_2^z \rangle /3. \tag{11}$$

Parallel spins give lower energy due to the opposite signs of spin densities. The $s = 1/2$ result is $-19/54 = -0.351\,85$ per site in first order and $-0.390\,82$ in second order in V, very close to the DMRG result of $-0.393\,85$ in Fig. 4. The $s = 1$ result is $-9/8 = -1.125$ per site in first order and -1.3152 in second order, slightly below -1.2796 in DMRG. The variational theorem holds for the energy in first order, but not in second order. The first-order energy is lowest for parallel spins of $N_B(g)$ trimers and site q that properly gives $S^z = S(q)s$. Moreover, $\Psi^{(0)}(q,g)$ immediately rationalizes low-energy spin flips in states with $S < S(g)$ for either $s = 1/2$ or 1 sites.

Site q is a NN of one middle site when q is in generation g and of three middle sites otherwise. The second term of Eq. (12) is more negative for $q \leqslant g - 2$ than for $q = g$ by $2\langle s_2^z \rangle (s - \langle s_1^z \rangle)$ for $s = 1/2$ or 1. To first order in V, site q is not on the boundary and g, $g - 1$ in Fig. 1 are trimers with end sites g. H_0 accounts for all exchanges between generations g and $g - 1$ while V contains all exchanges between $g - 1$ and $g - 2$. The trimer approximation leads to $\langle s_g^z \rangle = 1/3$ and $\langle s_{g-1}^z \rangle = -1/6$, compared to 0.40 and -0.25 for DMRG for $s = 1/2$ sites in Table II. The correlation functions are $\langle \vec{s}_{g-1} \cdot \vec{s}_g \rangle = -1/2$ compared to -0.44 for DMRG. Trimers have reduced $\langle \vec{s}_{g-2} \cdot \vec{s}_{g-1} \rangle = -1/18$, well below the DMRG result of -0.30 but consistent with reduced correlation in $g - 1$ and $g - 2$. The $s = 1$ BL has $\langle s_g^z \rangle = 3/4$ and $\langle s_{g-1}^z \rangle = -1/2$ in the trimer approximation and 0.87 and -0.69 in DMRG (Table II). Trimers have $\langle \vec{s}_{g-1} \cdot \vec{s}_g \rangle = -3/2$ for $s = 1$ while DMRG gives -1.397.

A trimer of $s = 1/2$ sites must be excited to a quartet state $s = 3/2$ with excitation energy 3/2 under H_0 to obtain $S^z = S(g) + 1$. One of the $N_B(g)$ trimers in $\Psi^{(0)}(q,g)$ is changed to $|\phi\rangle = |\alpha\alpha\alpha\rangle$. A normalized function with a quartet is

$$|\Phi(g)\rangle = [N_B(g)]^{-1/2} \sum_{m=1}^{N_B(g)} |\phi_m\rangle |\Psi^{(0)}(q,g)\rangle / |\psi_m\rangle. \tag{12}$$

The quartet is delocalized over the BL by the s^+s^- terms of V. To first order in V, the excitation energy to $S = S(g) + 1$ is

$$\langle \Phi|H|\Phi\rangle - \langle \Psi^{(0)}|H|\Psi^{(0)}\rangle = \Delta^{(1)} = 1.0. \tag{13}$$

Delocalization lowers the energy by 2/3 while the diagonal $s^z s^z$ contribution raises the energy by 1/6. The net effect is to lower the excitation from 3/2 to 1 for $s = 1/2$, somewhat above $\Delta = 0.74$ for the extended BL in Fig. 5.

The sharp distinction between NN exchanges in H_0 and V for the outermost three generations is lost in the interior. H_0 contains trimers that spans three generations when $q \leqslant g - 2$. When $q \neq 0$, the central site in Fig. 1 is the middle site of a trimer for even g and the end site for odd g. Although trimers imply intermediate spin density and spin correlations near the focal point, there are variations between even and odd g in contrast to identical $\langle s_0^z \rangle$ in Fig. 6. Similarly, $C(r)$ in Eq. (5) for $\Psi^{(0)}(q,g)$ is strictly limited to $r = 1$ or 2 since trimers span at most span three generations. The function $\Psi^{(0)}(q,g)$ is localized, more localized than the DMRG gs, but it rationalizes DMRG results in some detail.

DMRG results for NN exchange J in Eq. (1) for $s = 1/2$ and 1 sites in BL(3,3,g) are closely similar, in sharp contrast to the fundamentally different behavior of 1D chains of $s = 1/2$ and 1 sites.[26] The $s = 1$ chain with additional NN terms $J(s_i \cdot s_j)^2/3$ in Eq. (1) is a valence bond solid (VBS) with rigorously known gs properties.[27] The VBS on BL(3,3,g) has $s = 3/2$ sites, yet another added term to Eq. (1), and $\langle s_0^z \rangle = 0$, and hence no LRO in the extended system.[27] Both the spin and Hamiltonian of the VBS are different, and no DMRG has been performed on that system. For Eq. (1), DMRG indicates a gs with staggered magnetization and finite $\langle s_0^z \rangle$ in Fig. 6 at the focal point for either $s = 1/2$ or 1. The gs has LRO and short-range spin correlations $C(r)$ in Eq. (5) that decrease

exponentially and more rapidly than the number of boundary sites.

V. CONCLUSIONS

The DMRG algorithm in Sec. II makes it possible to treat the BL in Fig. 1 with $s = 1$ sites. It improves the accuracy for $s = 1/2$ sites and yields low-energy excitations. All DMRG results for either $s = 1/2$ or 1 sites can be understood qualitatively in terms of a trimer model for BL$(3,3,g)$.

Preliminary results for BL$(3,3,g)$ with $s = 3/2$ sites are satisfactory. The addition of a focal point with p degrees of freedom at each step can be used for BLs with more arms $b > 3$ or higher connectivity $Z > 3$, although with steep increases of computational resources. The bottleneck is the dimension $m^{Z-1} \times p$ of the block whose density matrix is constructed at each step; $m \approx 70$ for $Z = 3$ becomes $m \approx 17$ for $Z = 4$, which has limited accuracy. A comparable reduction to $m \approx 20$–30 limited previous algorithms[22–24] for BL$(3,3,g)$ to $s = 1/2$ sites. The dimension $m^b \times p$ of the superblock is less serious because only a few eigenvalues are required at each step.

ACKNOWLEDGMENTS

M.K. thanks S. R. White for discussion and B. J. Topham for reading the manuscript carefully. We thank the National Science Foundation for partial support of this work through the Princeton MRSEC (DMR-0819860).

*manoranj@princeton.edu

[1] D. A. Tomalia and P. R. Dvornic, Nature (London) **372**, 617 (2002).
[2] M. A. Martin-Delgado, J. Rodriguez-Laguna, and G. Sierra, Phys. Rev. B **65**, 155116 (2002).
[3] R. Esfand and D. A. Tomalia, Drug Discov. Today **6**, 427 (2001).
[4] S. Serroni, S. Campagna, F. Puntoriero, C. Di Pietro, N. D. McClenaghan, and F. Loiseau, Chem. Soc. Rev. **30**, 367 (2001).
[5] H. Frey, C. Lach, and K. Lorenz, Adv. Mater. **10**, 279 (1998).
[6] C. Dufes, I. F. Uchegbu, and A. G. Schatzlein, Adv. Drug Deliv. Rev. **57**, 2177 (2005).
[7] H. Kobayashi, S. Kawamoto, and S. K. Jo, Cancer Res. **63**, 271 (2003).
[8] A. W. Freeman, R. H. Vreekamp, and J. M. J. Fréchet, Polym. Mater. Sci. Eng. **77**, 138 (1997).
[9] A. A. Ovchinnikov, Theoret. Chim. Acta **47**, 297 (1978).
[10] E. H. Lieb, Phys. Rev. Lett. **62**, 1201 (1989); E. H. Lieb and D. Mattis, J. Math. Phys. **3**, 749 (1962).
[11] A. Georges and G. Kotliar, Phys. Rev. B **45**, 6479 (1992).
[12] C. R. da Silva and S. Coutinho, Phys. Rev. B **34**, 7975 (1986).
[13] J. B. Salzberg, L. M. Falicov, and C. E. T. Gonalves da Silva, Solid State Commun. **18**, 1077 (1976).
[14] P. M. Bleher, Commun. Math. Phys. **128**, 411 (1990).
[15] D. Dhar, P. Shukla, and J. P. Sethna, J. Phys. A **30**, 5259 (1997).
[16] D. J. Scalapino, S. R. White, and S. C. Zhang, Phys. Rev. Lett. **68**, 2830 (1992); Phys. Rev. B **47**, 7995 (1993).
[17] S. R. White, Phys. Rev. B **48**, 10345 (1993); U. Schollwöck, Rev. Mod. Phys. **77**, 259 (2005); K. Hallberg, Adv. Phys. **55**, 477 (2006).
[18] M. Kumar, Y. A. Pati, and S. Ramasesha, J. Chem. Phys. **136**, 014112 (2012).
[19] S. Yan, D. A. Huse, and S. R. White, Science **332**, 1173 (2011); U. Schollwöck, Int. J. Mod. Phys. B **21**, 2564 (2007).
[20] M. Kumar, Z. G. Soos, D. Sen, and S. Ramasesha, Phys. Rev. B **81**, 104406 (2010); M. Kumar, S. Ramasesha, and Z. G. Soos, *ibid.* **79**, 035102 (2009); C. Raghu, Y. Anusooya Pati, and S. Ramasesha, *ibid.* **66**, 035116 (2002).
[21] M. Kumar, S. Ramasesha, D. Sen, and Z. G. Soos, Phys. Rev. B **75**, 052404 (2007).
[22] H. Otsuka, Phys. Rev. B **53**, 14004 (1996).
[23] B. Friedman, J. Phys.: Condens. Matter **9**, 9021 (1997).
[24] M. B. Lepetit, M. Cousy, and G. M. Pastor, Eur. Phys. J. B **13**, 421 (2000).
[25] U. Schollwöck, Ann. Phys. **326**, 96 (2011).
[26] F. D. M. Haldane, Phys. Lett. A **93**, 464 (1983).
[27] I. Affleck, T. Kennedy, E. H. Lieb, and H. Tasaki, Commun. Math. Phys. **115**, 477 (1988).